

# Proteome-wide Analysis of Cellular Response to Ultraviolet Light for Biomaterial Synthesis and Modification

Emily R. Ruskowitz<sup>†</sup> and Cole A. DeForest<sup>\*,†,‡,§,⊥</sup>

<sup>†</sup>Department of Chemical Engineering, <sup>‡</sup>Department of Bioengineering, and <sup>§</sup>Molecular Engineering & Sciences Institute, University of Washington, Seattle, Washington 98195, United States

<sup>⊥</sup>Institute of Stem Cell & Regenerative Medicine, University of Washington, Seattle, Washington 98109, United States

## Supporting Information



**ABSTRACT:** Though the biomaterials community has widely utilized near-ultraviolet (UV) light to make and modify scaffolds for 3D cell culture, thorough examination of the downstream effects of such light on cell function has not been performed. Here, we investigate the global effects of common light treatments on NIH3T3 fibroblasts and human mesenchymal stem cells (hMSCs), cell types regularly employed in tissue engineering. Unchanged proliferation rates, an absence of apoptotic induction, and an unaltered proteome following low-dose 365 nm light exposure are observed, implying that near-UV-based radical-free photochemistries can be exploited in biomaterial systems without deleteriously affecting cell fate.

**KEYWORDS:** proteomics, photochemistry, UV light, stimuli, photoresponsive biomaterials

Photochemistries uniquely enable spatiotemporal control over biomaterial formation and chemical/physical modification,<sup>1</sup> providing powerful strategies to probe and direct dynamic bioprocesses *in vitro*.<sup>2</sup> Among many examples, light-induced reactions have been utilized to irreversibly degrade hydrogels,<sup>1</sup> covalently decorate materials with proteins,<sup>3</sup> and activate immunomodulatory peptide presentation *in vivo*.<sup>4</sup> Photoreactions are unique in that they can be confined to specific 4D locations (i.e., 3D space and time) designated by when and where photons are delivered to the sample. Theoretically limited only by the wavelength of utilized light, photochemical patterning resolution ( $\sim 1 \mu\text{m}$ ) is much smaller than the size of a single cell ( $\sim 10 \mu\text{m}$ ), enabling reactions to be controlled over virtually all biologically relevant length scales.<sup>5,6</sup>

For photochemically modulated biomaterial systems involving living cells, wavelength selection represents a careful balance of several factors: photons must possess high enough energy to induce the intended reactions but not so much to incur oxidative stress or DNA mutations.<sup>7</sup> Though a suite of chemistries efficiently react to middle-UV light ( $\lambda = 200\text{--}300 \text{ nm}$ , typically 254 nm), exposure to these high-energy wavelengths are widely accepted to damage cells through the

production of DNA lesions in the form of cyclobutane pyrimidine dimers and pyrimidine-pyrimidone (6–4) photo-products.<sup>7</sup> As such, the biomaterials community has gravitated toward using near-UV light ( $\lambda = 300\text{--}400 \text{ nm}$ , most commonly 365 nm) to initiate reactions in the presence of living cells. Despite this regular utilization, there is lingering concern that such near-UV light exposure may induce damage through generation of reactive oxygen species (ROS)<sup>8,9</sup> or DNA oxidation.<sup>10</sup> Such long-term mutagenic effects can potentially be mitigated through cell cycle arrest and repair pathways through excision and replacement of damaged DNA prior to further replication.<sup>11</sup> Given the cell's endogenous propensity to repair possible UV-induced damage, in-depth analyses of the functional state of cells downstream of treatment is necessary to understand the long-term effects of near-UV light exposure, particularly in a biomaterials' context.

Though some information is known about light's wavelength-dependent effects on DNA chemistry, perhaps more important is how such possible changes carry forward and

**Received:** February 4, 2019

**Accepted:** March 31, 2019

**Published:** April 5, 2019

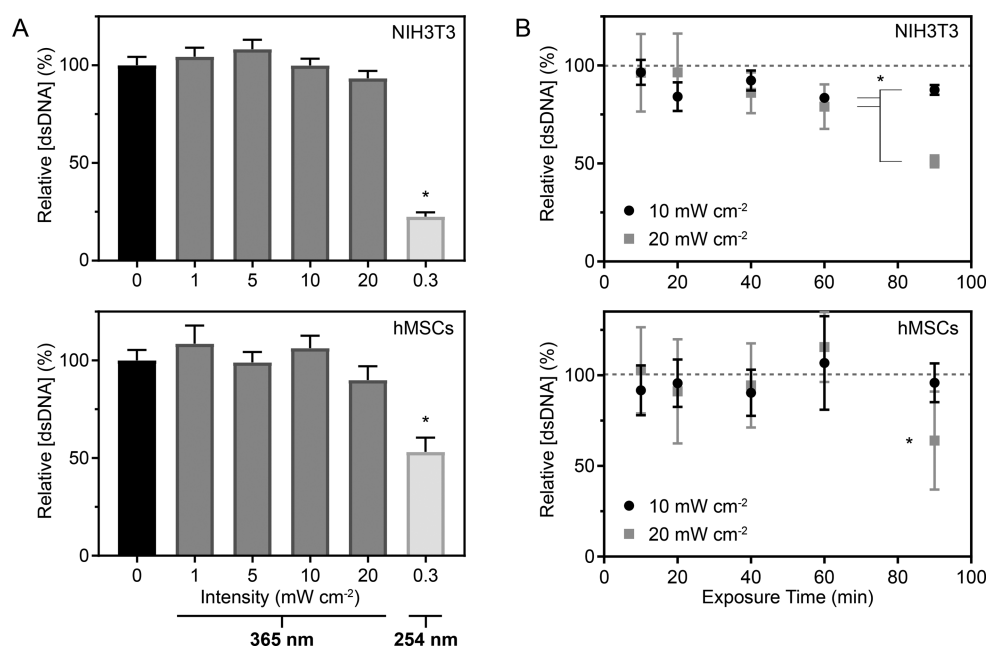


**Figure 1.** (A) Cell proliferation was quantified 24 h after light treatment (10 min for  $\lambda = 365$  nm or 0.5 min for  $\lambda = 254$  nm) at varied intensities ( $0\text{--}20$  mW cm<sup>-2</sup>) for (top) NIH3T3s and (bottom) hMSCs using the PicoGreen Assay. (B) Similarly, the effects of prolonged near-UV exposure (10–90 min for  $\lambda = 365$  nm at 10 and 20 mW cm<sup>-2</sup>) on proliferation of (top) NIH3T3s and (bottom) hMSCs was quantified. \* corresponds to statistically significant differences in observed values ( $p < 0.01$ ,  $t$ -test) relative to unexposed controls. Error bars correspond to  $\pm 1$  standard deviation about the mean for  $n \geq 4$  biological replicates.

manifest throughout transcription and translational processes. Although mRNA is directly translated into proteins, regulatory and post-translational processes hinder direct correlation between gene and protein abundance, necessitating measures of the key communicatory space, the proteome.<sup>12</sup> Current high-throughput proteomic tools permit quantitative, in-depth investigations into cell response downstream of stimuli. These techniques can provide a highly precise understanding of proteomic shifts in response to environmental perturbations or well-defined treatments with no prior prediction of the mechanisms of action. One such technique, pulsed stable isotope labeling by amino acids in cell culture (pSILAC), provides quantitative, comparative information between treated and untreated populations by incorporating isotopically heavy labels into newly translated proteins. Relative label abundance within each protein species, as determined through liquid chromatography coupled to tandem mass spectrometry (LC-MS/MS), offers a high-throughput approach to understand how treatment globally influences protein production. Such experiments provide deeper insight into common practices that may otherwise bias experimental results. This manuscript highlights new findings on the proteomic response of multiple cell lines to UV light at dosages highly relevant in the synthesis and modification of biomaterials.

Even with its frequent utilization in biomaterials, studies investigating the cellular response to narrow band-pass, near-UV light are limited. Cytocompatibility has primarily been determined through simple proliferation assays at conditions common within biomaterials ( $\lambda = 365$  nm,  $\sim 10$  mW cm<sup>-2</sup>, 10 min).<sup>13,14</sup> More recently, the Kasko group investigated the effects of low-dose, near-UV light on hMSC function and found no significant change in global gene expression after multiple exposures totaling 25 min at  $\lambda = 300\text{--}425$  nm ( $3.5$  mW cm<sup>-2</sup>);<sup>15</sup> though this was a substantial finding, the broad-range light exposures and repetitive dosing does not mimic the

most common photoconditions used to modify biomaterials, leaving open questions concerning the effects of more typical treatments on cell fate.

Herein, we sought to examine the downstream effects on cellular phenotype after exposure to UV light using global quantitative proteomic techniques. NIH3T3 mouse fibroblasts and hMSCs, two highly utilized cell types in 3D cell culture and material development that differ in proliferation rate and sensitivity, were maintained at 37 °C and 5% CO<sub>2</sub> on tissue-culture polystyrene T-75 flask (Genesee Scientific). NIH3T3s were cultured in Dulbecco's Modified Eagle Media (Thermo Fisher Scientific) containing glucose ( $4.5$  g L<sup>-1</sup>) supplemented with fetal bovine serum (FBS, 10%, Corning) and penicillin/streptomycin (PS, 1%, Corning), while hMSCs were maintained in complete MesenPRO RS medium (Thermo Fisher Scientific). Cells were seeded on six-well tissue culture polystyrene plates (Genesee Scientific) for 24 h prior to exchanging media with Dulbecco's phosphate-buffered saline containing magnesium and calcium (DPBS, Corning) and subsequent light treatment. Cells were exposed to collimated near-UV light ( $\lambda = 365$  nm; 10 min at 1, 5, 10, and 20 mW cm<sup>-2</sup>; Omnicure 1500) equipped with a 360 nm cutoff filter (Omega Optical Inc.) or middle-UV ( $\lambda = 254$  nm, 0.5 min at 0.3 mW cm<sup>-2</sup>, UVP Mineralight UVGL-25) before swapping back to complete media. The addition of a 360 nm cutoff filter acts as an engineered control to eliminate lower wavelengths due to possible light-source filter degradation or the natural bell-curve emission spectra of a mercury lamp.

To determine if light exposures altered cellular growth rate, proliferation was quantified (PicoGreen Assay, Molecular Probes) 24 h after light exposure. No significant changes in proliferation were found after 365 nm light treatments (10 min at 1, 5, 10, and 20 mW cm<sup>-2</sup>) in either NIH3T3s or hMSCs (Figure 1A) as compared with unexposed controls. In contrast, 254 nm treatments (0.5 min at 0.3 mW cm<sup>-2</sup>) significantly

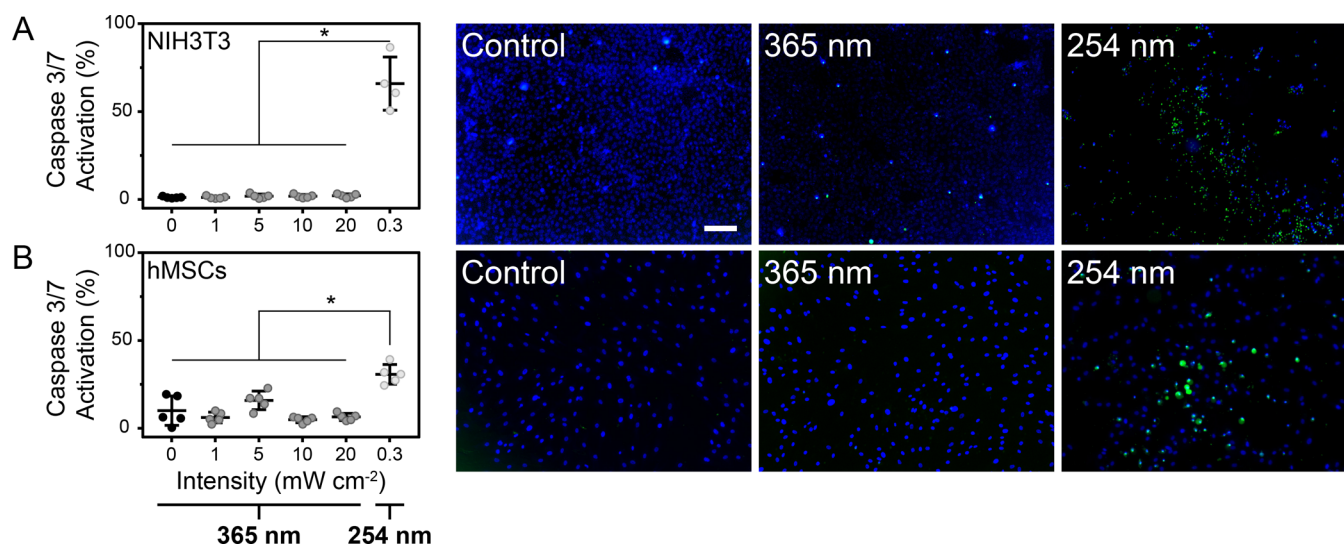


**Figure 2.** Apoptotic activation of (A) NIH3T3s and (B) hMSCs 24 h after light treatment (10 min for  $\lambda = 365$  nm or 0.5 min for  $\lambda = 254$  nm) at varied intensities (0–20 mW cm<sup>-2</sup>). Activation was quantified through colabeling with CellEvent Caspase-3/7 (green) and Hoechst 33342 nuclear stain (blue). Percent activation was calculated as the ratio of caspase-3/7-positive cells (green) relative to the total number of cells (blue). Representative fluorescent images highlight significant activation following 254 nm light exposure (0.3 mW cm<sup>-2</sup>, 0.5 min), as well as a lack of apoptosis in 365 nm treated (10 mW cm<sup>-2</sup>, 10 min) and unexposed control samples ( $p < 0.01$ ). Error bars in column scatter plots correspond to  $\pm 1$  standard deviation about the mean for  $n \geq 4$  biological replicates. Scale bar = 250  $\mu$ m.

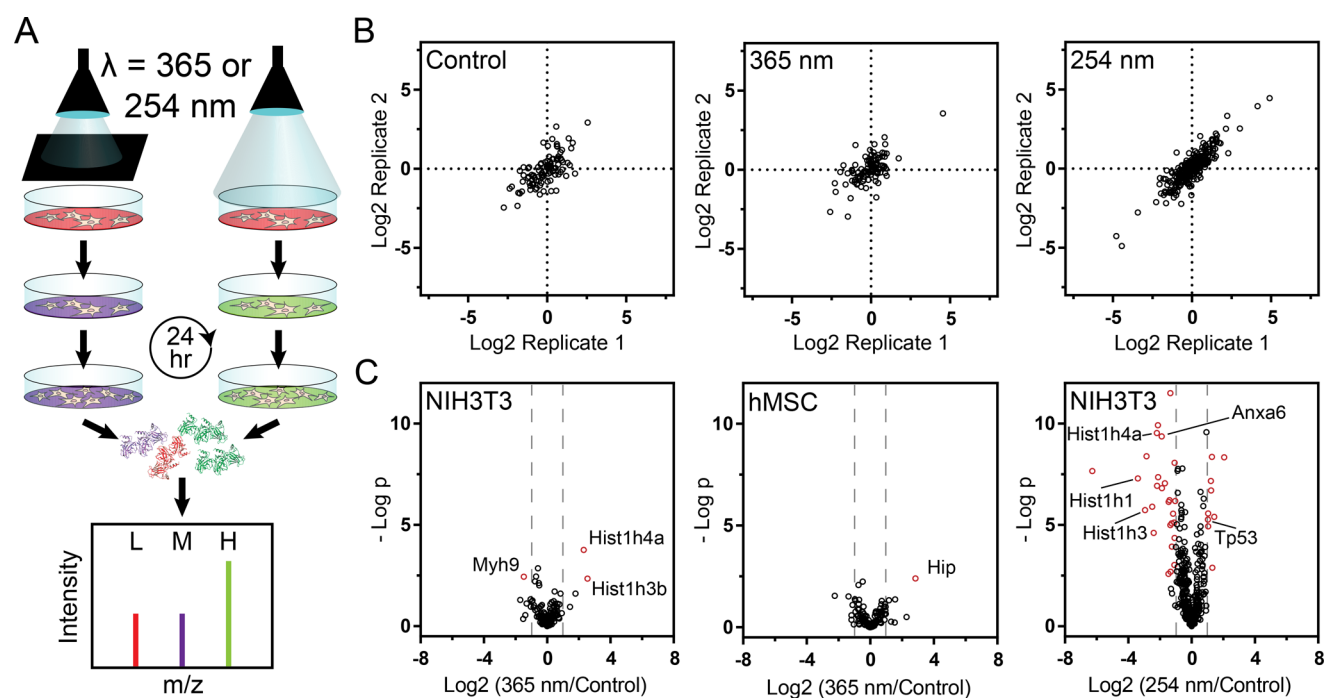


**Figure 3.** Quantification of the global proteomic response to UV light in cell culture. (A) Pulsed stable isotopic labeling by amino acids in cell culture (pSILAC) permitted quantification of newly synthesized proteins after treatment with 254 nm (0.3 mW cm<sup>-2</sup>, 0.5 min) or 365 nm light (10 mW cm<sup>-2</sup>, 10 min). Relative protein expression was determined by combining treated samples with an unexposed control sample, digesting proteins into peptide fragments, and processing LC-MS/MS spectra. (B) Representative correlations of the relative protein expression ( $\log_2$  treated/untreated) demonstrate consistent response in NIH3T3 label-swapped biological replicates. (C) Treated samples were compared to controls to determine statistically significant differences in newly expressed proteins. Proteins with ratios significantly different (two-sided  $t$ -test with a false discovery rate of 0.01) from 1 are indicated by red circles. Vertical dashed lines indicate a protein ratio of  $\pm 2$ .

decreased proliferation in both cell types, suggesting that middle-UV yielded irreparable DNA damage resulting in cell death or cell-cycle arrest. To further investigate an acceptable threshold of exposure of near-UV light, studies were extended to larger dosages ( $\lambda = 365$  nm, 10–90 min at 10 and 20 mW cm<sup>-2</sup>). Experiments revealed that hMSC proliferation is not

affected with statistical significance ( $p < 0.01$ ) until being exposed to near-UV light at 20 mW cm<sup>-2</sup> for  $\geq 90$  min; NIH3T3 proliferation decreased slightly after  $\geq 60$  min of exposure (Figure 1B). These findings imply that the short exposures traditionally employed to photochemically control biomaterial properties do not affect cell function, though the

decreased proliferation observed with very high light dosages motivates a deeper analysis of intracellular response under more typical exposure conditions.

UV light is known to initiate pro-apoptotic pathways after the production of DNA photoproducts and in response to UV-induced oxidative stress.<sup>16</sup> Apoptotic pathways converge to the activation of downstream executioner caspases-3, -6, and -7 prior to programmed cell death.<sup>17</sup> To determine if apoptotic damage accompanied the selected treatments ( $\lambda = 365$  nm, 10 min at 1, 5, 10, and 20 mW cm<sup>-2</sup>;  $\lambda = 254$  nm, 0.5 min at 0.3 mW cm<sup>-2</sup>), we quantified caspase-3/7 activation 24 h after UV exposure by determining the percentage of activated cells (CellEvent, green) relative to total cell count (Hoechst 33342, blue) after staining and fluorescent imaging (Figure 2). In agreement with results from proliferation assays, NIH3T3s and hMSCs exhibited a quantitative increase in caspase activation following 254 nm light treatment while cells treated with 365 nm light were statistically indistinguishable from unexposed controls ( $p < 0.01$ ). These findings indicate that light-induced apoptosis occurs in a wavelength-dependent manner, further emphasizing the importance of appropriately selecting light treatments when working with photoresponsive biomaterials.

With constant proliferation rates and an absence of apoptosis in either cell type, we employed high-throughput pSILAC to provide an in-depth analysis of global cell response of NIH3T3s and hMSCs to UV light. pSILAC offers quantification of all newly synthesized proteins, yielding insight into the processes occurring downstream of stimulation (Figure 3A).<sup>18</sup> On the basis of protein concentrations (BCA assay, ThermoFisher), two protein samples generated using different isotopic labels are combined at a 1:1 ratio to quantify variations in protein synthesis after light treatment. Here, we incorporated a lysine isotope into the proteome by swapping the growth medium to that containing either a “medium heavy” (D4-L-lysine, Cambridge Isotope Laboratories) or “heavy” (<sup>13</sup>C<sub>6</sub><sup>15</sup>N<sub>2</sub>-L-lysine, Cambridge Isotope Laboratories) L-lysine hydrochloride (146 mg L<sup>-1</sup> equivalents) for 24 h after exposure to either 365 nm light at 10 mW cm<sup>-2</sup> or 254 nm light at 0.3 mW cm<sup>-2</sup> (Figure 3A). Three biological replicates, including label-swap experiments, were collected for each treatment condition. Proteins were further purified and digested with the endopeptidase LysC (Wako Chemicals) to produce singly labeled peptides for quantification through LC-MS/MS (Supporting Information).

Acquired raw data were processed using the MaxQuant<sup>19</sup>/Andromeda<sup>20</sup> platform (v.1.5.3.30) under default settings (Supporting Information) to provide quantitative results reported here as treated/control (H/M or M/H) or fold change. Further data interpretation was performed on the normalized protein ratios, which accounts for unequal mixing or loading, in Perseus (v.1.6.1.2), a software platform to analyze quantitative proteomic data.<sup>21</sup> First, data was filtered for false detections, contaminants, and proteins detected by a single site. Stringent filtering for proteins detected in less than 70% of the replicates were then removed, leaving 383 and 153 unique proteins in the NIH3T3 and hMSC data sets, respectively. Filtered data was then log<sub>2</sub> transformed to center fold changes in protein expression around 0 (Figure S1). Representative NIH3T3 biological replicates (Figure 3B) from the control and 365 nm groups clustered primarily around 0 while 254 nm samples correlated highly (average Pearson value of 0.90). In contrast to 254 nm light where changes were reproducibly detected, these trends indicate that 365 nm UV

light exposure does not substantially shift protein production or alter the proteome.

Data sets were further analyzed for differentially regulated proteins after light exposure. To determine statistical significance, treatment replicates were grouped and compared to control samples using a two-sided *t*-test with the false discovery rate set to 0.01 (Figure 3C). Proteins resulting in a 2-fold change in expression following treatment were considered significant. In NIH3T3s, only three proteins exhibited differential expression values after exposure to 365 nm light: the Myosin-9 motor-protein and potential marker of metastasis<sup>22</sup> was downregulated 2.8-fold, whereas histones-H3.2 and -H4 were upregulated 6.1- and 13.9-fold, respectively. These core histones are structural proteins essential in nucleosomes that have shown fluctuation in gene expression correlating to cell-cycle phases.<sup>23</sup> Although specific function of these histones is extremely dependent on post-translational modifications, UV-induced DNA damage (254 nm) initiates chromatin relaxation and localized H4 reduction within minutes to facilitate repair pathways.<sup>24–26</sup> As no up-regulation in key downstream markers associated with UV-induced DNA damage was detected for 365 nm exposure, we attribute the observed upregulation to slight differences in cell phase. For hMSCs, a single chaperone protein, heat-shock protein-70 interacting protein (Hip), was found to be upregulated 6.9-fold following 365 nm treatment (Figure 3C). Although Hip may take part in regulation of proliferation and apoptosis, very little experimental data exists to correlate expression changes to physiologic changes and proliferation and apoptosis rates matched control samples (Figures 1 and 2B).<sup>27</sup> As these data indicate that near-UV 365 nm light does not induce significant proteomic shifts or activation of specific pathways, it can be considered cytocompatible.

In agreement with proliferation and apoptosis assays, middle-UV 254 nm light treatment significantly shifted protein expression in NIH3T3 cells (Figure 3C). 40 proteins were differentially expressed 24 h after 254 nm light (Table S1). Included in this list were histones-H1.2, -H2A, -H3.2, and -H4, which were found to be significantly down-regulated, and cellular tumor protein p53, which was among the 10 up-regulated proteins. DNA damage induced by ionizing radiation represses histone expression in a p53-dependent manner.<sup>28</sup> Additionally, further analysis using the STRING functional protein association network database<sup>29</sup> suggests its significant downregulation in metabolic pathways ( $p < 0.005$ ). These results corroborate expected damage caused by 254 nm light.

The unique ability to direct light exposure near-instantaneously in 4D has enabled the development of materials for triggered drug delivery and advanced cell culture. To fully translate these systems into biological settings, complete knowledge of the biological impact of each of its element, including light dosage, is essential. Here, we provide a vital investigation of the biological impact of low-dose UV light treatments regularly used to control photochemistries in biomaterials. Proliferation rates remained unchanged and apoptosis was not induced after exposure to varied intensities of 365 nm light in two cell types; meanwhile, cells were significantly altered by exposure to lower wavelength UV light. Using pSILAC, we looked deeper for initiation of common repair pathways or any signal of cellular damage following treatment through analysis of the proteome and again found no significant changes in response to 365 nm light. Combined, low doses of 365 nm light are safe for application in a

biological setting. However, the varied response to 254 nm light between NIH3T3s and hMSCs suggests a cell-line dependent sensitivity. This work gives credence to the further utilization of radical-free near-UV photochemistry in creation and modification of biomaterial systems without deleteriously affecting cell fate.

## ■ ASSOCIATED CONTENT

### 📄 Supporting Information

The Supporting Information is available free of charge on the ACS Publications website at DOI: [10.1021/acsbomaterials.9b00177](https://doi.org/10.1021/acsbomaterials.9b00177).

Proliferation and apoptosis assay protocols, methods for pSILAC experiments, proteomic data distributions, tabulated differentially expressed proteins after 254 nm light exposure (PDF)

## ■ AUTHOR INFORMATION

### Corresponding Author

\*Email: [profcole@uw.edu](mailto:profcole@uw.edu).

### ORCID

Cole A. DeForest: [0000-0003-0337-3577](https://orcid.org/0000-0003-0337-3577)

### Author Contributions

The manuscript was written through contributions of all authors. All authors have given approval to the final version of the manuscript.

### Funding

This work was supported by a grant from the National Science Foundation (CBET CBE 1803054, C.A.D.) and a Royalty Research Fund Grant (C.A.D.) from the University of Washington.

### Notes

The authors declare no competing financial interest.

## ■ ACKNOWLEDGMENTS

This work is supported in part by the University of Washington's Proteomics Resource (UWPR95794). The authors gratefully acknowledge technical input from C. Arakawa, C. Barnes, S. Ong, and P. von Haller. Protein structures in Figure 3A and the Table of Contents graphic were acquired from RCSB Protein Data Bank and modified with UCSF Chimera.

## ■ ABBREVIATIONS

UV, ultraviolet; pSILAC, pulsed stable isotope labeling by amino acids in cell culture; LC-MS/MS, liquid chromatography tandem mass spectrometry; ROS, reactive oxygen species

## ■ REFERENCES

- (1) Kloxin, A. M.; Kasko, A. M.; Salinas, C. N.; Anseth, K. S. Photodegradable Hydrogels for Dynamic Tuning of Physical and Chemical Properties. *Science* **2009**, *324* (5923), 59–63.
- (2) Ruskowitz, E. R.; DeForest, C. A. Photoresponsive Biomaterials for Targeted Drug Delivery and 4D Cell Culture. *Nat. Rev. Mater.* **2018**, *3* (2), 17087.
- (3) DeForest, C. A.; Tirrell, D. A. A Photoreversible Protein-Patterning Approach for Guiding Stem Cell Fate in Three-Dimensional Gels. *Nat. Mater.* **2015**, *14* (5), 523–531.
- (4) Lee, T. T.; Garcia, J. R.; Paez, J. I.; Singh, A.; Phelps, E. A.; Weis, S.; Shafiq, Z.; Shekaran, A.; Del Campo, A.; Garcia, A. J. Light-Triggered In Vivo Activation of Adhesive Peptides Regulates Cell

Adhesion, Inflammation and Vascularization of Biomaterials. *Nat. Mater.* **2015**, *14* (3), 352–360.

(5) Arakawa, C. K.; Badeau, B. A.; Zheng, Y.; DeForest, C. A. Multicellular Vascularized Engineered Tissues through User-Programmable Biomaterial Photodegradation. *Adv. Mater.* **2017**, *29* (37), 1703156.

(6) Adelmund, S. M.; Ruskowitz, E. R.; Farahani, P. E.; Wolfe, J. V.; DeForest, C. A. Light-Activated Proteomic Labeling via Photocaged Bioorthogonal Non-Canonical Amino Acids. *ACS Chem. Biol.* **2018**, *13* (3), 573–577.

(7) Pfeifer, G. P.; You, Y.-H.; Besaratinia, A. Mutations Induced by Ultraviolet Light. *Mutat. Res., Fundam. Mol. Mech. Mutagen.* **2005**, *571* (1–2), 19–31.

(8) Cadet, J.; Sage, E.; Douki, T. Ultraviolet Radiation-Mediated Damage to Cellular DNA. *Mutat. Res., Fundam. Mol. Mech. Mutagen.* **2005**, *571* (1–2), 3–17.

(9) Lawrence, K. P.; Douki, T.; Sarkany, R. P. E.; Acker, S.; Herzog, B.; Young, A. R. The UV/Visible Radiation Boundary Region (385–405 Nm) Damages Skin Cells and Induces “dark” Cyclobutane Pyrimidine Dimers in Human Skin In Vivo. *Sci. Rep.* **2018**, *8* (1), 12722.

(10) Kozmin, S.; Slezak, G.; Reynaud-Angelin, A.; Elie, C.; de Rycke, Y.; Boiteux, S.; Sage, E. UVA Radiation Is Highly Mutagenic in Cells That Are Unable to Repair 7,8-Dihydro-8-Oxoguanine in *Saccharomyces Cerevisiae*. *Proc. Natl. Acad. Sci. U. S. A.* **2005**, *102* (38), 13538–13543.

(11) Dunkern, T. R.; Fritz, G.; Kaina, B. Ultraviolet Light-Induced DNA Damage Triggers Apoptosis in Nucleotide Excision Repair-Deficient Cells via Bcl-2 Decline and Caspase-3/-8 Activation. *Oncogene* **2001**, *20* (42), 6026–6038.

(12) Vogel, C.; Marcotte, E. M. Insights into the Regulation of Protein Abundance from Proteomic and Transcriptomic Analyses. *Nat. Rev. Genet.* **2012**, *13* (4), 227–232.

(13) Bryant, S. J.; Nuttelman, C. R.; Anseth, K. S. Cytocompatibility of UV and Visible Light Photoinitiating Systems on Cultured NIH/3T3 Fibroblasts In Vitro. *J. Biomater. Sci., Polym. Ed.* **2000**, *11* (5), 439–457.

(14) Gerecht, S.; Burdick, J. A.; Ferreira, L. S.; Townsend, S. A.; Langer, R.; Vunjak-Novakovic, G. Hyaluronic Acid Hydrogel for Controlled Self-Renewal and Differentiation of Human Embryonic Stem Cells. *Proc. Natl. Acad. Sci. U. S. A.* **2007**, *104* (27), 11298–11303.

(15) Wong, D. Y.; Ranganath, T.; Kasko, A. M. Low-Dose, Long-Wave UV Light Does Not Affect Gene Expression of Human Mesenchymal Stem Cells. *PLoS One* **2015**, *10* (9), No. e0139307.

(16) Ikehata, H.; Kawai, K.; Komura, J.; Sakatsume, K.; Wang, L.; Imai, M.; Higashi, S.; Nikaido, O.; Yamamoto, K.; Hieda, K.; et al. UVA1 Genotoxicity Is Mediated Not by Oxidative Damage but by Cyclobutane Pyrimidine Dimers in Normal Mouse Skin. *J. Invest. Dermatol.* **2008**, *128* (9), 2289–2296.

(17) Budihardjo, I.; Oliver, H.; Lutter, M.; Luo, X.; Wang, X. Biochemical Pathways of Caspase Activation During Apoptosis. *Annu. Rev. Cell Dev. Biol.* **1999**, *15* (1), 269–290.

(18) Schwanhäusser, B.; Gossen, M.; Dittmar, G.; Selbach, M. Global Analysis of Cellular Protein Translation by Pulsed SILAC. *Proteomics* **2009**, *9* (1), 205–209.

(19) Cox, J.; Mann, M. MaxQuant Enables High Peptide Identification Rates, Individualized P.p.b.-Range Mass Accuracies and Proteome-Wide Protein Quantification. *Nat. Biotechnol.* **2008**, *26* (12), 1367–1372.

(20) Cox, J.; Neuhauser, N.; Michalski, A.; Scheltema, R. A.; Olsen, J. V.; Mann, M. Andromeda: A Peptide Search Engine Integrated into the MaxQuant Environment. *J. Proteome Res.* **2011**, *10* (4), 1794–1805.

(21) Tyanova, S.; Temu, T.; Sinitcyn, P.; Carlson, A.; Hein, M. Y.; Geiger, T.; Mann, M.; Cox, J. The Perseus Computational Platform for Comprehensive Analysis of (Pro)teomics Data. *Nat. Methods* **2016**, *13* (9), 731–740.

(22) Lund, R. R.; Terp, M. G.; Laenkholm, A.-V.; Jensen, O. N.; Leth-Larsen, R.; Ditzel, H. J. Quantitative Proteomics of Primary Tumors with Varying Metastatic Capabilities Using Stable Isotope-Labeled Proteins of Multiple Histogenic Origins. *Proteomics* **2012**, *12* (13), 2139–2148.

(23) Chrysogelos, S.; Riley, D. E.; Stein, G.; Stein, J. A Human Histone H4 Gene Exhibits Cell Cycle-Dependent Changes in Chromatin Structure That Correlate with Its Expression. *Proc. Natl. Acad. Sci. U. S. A.* **1985**, *82* (22), 7535–7539.

(24) Hauer, M. H.; Gasser, S. M. Chromatin and Nucleosome Dynamics in DNA Damage and Repair. *Genes Dev.* **2017**, *31* (22), 2204–2221.

(25) Luijsterburg, M. S.; Lindh, M.; Acs, K.; Vrouwe, M. G.; Pines, A.; van Attikum, H.; Mullenders, L. H.; Dantuma, N. P. DDB2 Promotes Chromatin Decondensation at UV-Induced DNA Damage. *J. Cell Biol.* **2012**, *197* (2), 267–281.

(26) Adam, S.; Dabin, J.; Chevallier, O.; Leroy, O.; Baldeyron, C.; Corpet, A.; Lomonte, P.; Renaud, O.; Almouzni, G.; Polo, S. E. Real-Time Tracking of Parental Histones Reveals Their Contribution to Chromatin Integrity Following DNA Damage. *Mol. Cell* **2016**, *64* (1), 65–78.

(27) Shi, Z.; Zhang, J.; Zheng, S. What We Know about ST13, a Co-Factor of Heat Shock Protein, or a Tumor Suppressor? *J. Zhejiang Univ., Sci., B* **2007**, *8* (3), 170–176.

(28) Su, C.; Gao, G.; Schneider, S.; Helt, C.; Weiss, C.; O'Reilly, M. A.; Bohmann, D.; Zhao, J. DNA Damage Induces Downregulation of Histone Gene Expression through the G1 Checkpoint Pathway. *EMBO J.* **2004**, *23* (5), 1133–1143.

(29) Szklarczyk, D.; Morris, J. H.; Cook, H.; Kuhn, M.; Wyder, S.; Simonovic, M.; Santos, A.; Doncheva, N. T.; Roth, A.; Bork, P.; et al. The STRING Database in 2017: Quality-Controlled Protein–protein Association Networks, Made Broadly Accessible. *Nucleic Acids Res.* **2017**, *45* (D1), D362–D368.